LBL-10547

Lawrence Berkeley Laboratory
UNIVERSITY OF CALIFORNIA

Engineering & Technical
Services Division

Presented at the Deep Underwater Muon and Neutrino Detection Signal Processing Workshop, DUMAND Hawaii Center, University of Hawaii, Honolulu, February 11-16, 1980

PHOTOMULTIPLIER CHARACTERISTICS CONSIDERATIONS FOR THE DEEP UNDERWATER MUON AND NEUTRINO DETECTION SYSTEM

Branko Leskovar

February 1980

Prepared for the U.S. Department of Energy under Contract W-7405-ENG-48

Presented at the Deep Underwater Muon and Neutrino Detection Signal Processing Workshop, DUMAND Hawaii Center, University of Hawaii, Honolulu, February 11-16, 1980

LBL-10547

PHOTOMULTIPLIER CHARACTERISTICS CONSIDERATIONS FOR THE DEEP UNDERWATER MUON AND NEUTRINO DETECTION SYSTEM

Branko Leskovar

February 23, 1980

Prepared for the U. S. Department of Energy
under Contract W-7405-ENG-48

secondary emission gain increases linearly with increasing primary energy up to very high voltages.

Secondary-emission yields of the GaP(Cs) surface are considerably higher, typically between 30 and 50 at a primary electron energy of 600 eV, than those obtained with conventional dynode materials, where average dynode gains of 5 to 8 can be achieved[6,7]. Because the electron resolution of a photomultiplier depends primarily upon the average gain of the first dynode and the distribution in a number of secondary electrons, a higher electron resolution has been achieved, together with better dark-pulse distribution, decreased anode pulse rise time due to the fewer number of stages, and increased time resolution capabilities. Consequently, photomultipliers having dynodes with a GaP(Cs) secondary emitting surface are suitable for low-energy scintillation counting and for generating signals required in certain experimental research areas, where the device used for generating signals should absorb a minimum energy from the particles being studied, having at the same time very small spurious signal response.

Concerning the multiple-particle pulse-height resolution capabilities of a photomultiplier, the output pulse distribution has sharply defined peaks, if the statistical distribution of the secondary emission from dynodes follows closely a Poisson distribution. However, the observed distributions for secondary electrons vary, for different types of dynodes, from an exponential distribution to a Poisson distribution. To describe the wide variety of distributions, the Polya or negative binomial distribution for dynode secondary emission statistics has been successfully applied[8,9]. The Polya distribution is defined by the expression

$$P(x) = \frac{\mu^x}{x!} (1+b\mu)^{-x-1/b} \prod_{i=1}^{x-1} (1+ib) \qquad (2)$$

where $P(x)$ is the probability of observing x secondary electrons, μ is the mean value of distribution, and b is a parameter controlling the shape of the distribution. In the case of $b = 0$, the Polya distribution reduces to a Poisson distribution:

$$P(x)_0 = \frac{\mu^x}{x!} e^{-u} \qquad (3)$$

For $b = 1$, the Polya distribution reduces to an exponential distribution as a

special case:

$$P(x)_1 = \mu^x(1+\mu)^{-(x+1)} \tag{4}$$

Consequently, a Polya distribution as a model for dynode secondary emission statistics is capable of representing a wide range of shapes of secondary electron distributions because it contains as special extreme cases both the Poisson and exponential distributions. More specifically, numerically calculated values of the single electron spectrum, using Polya distribution as a model for dynode statistics, show how the electron distribution changes continuously from a distinctively Poisson peak in the b = o limit to an expontial distribution in the b = 1 limit[7]. As a matter of fact, for b ≥ 0.5 the distribution is approaching the exponential distribution, because the peak of the distribution moves to small pulse heights and the distribution itself has a long quasi-exponential tail.

The generating function of the Polya distribution is given by the relation:

$$Q(s) = [1 + b\mu\ (1-s)]^{-1/b} \tag{5}$$

Hence, the mean value and the variance of the distribution are

$$\bar{n} = \left.\frac{\delta Q(s)}{\delta s}\right|_{s=1} = \left.\frac{\delta[1+b\mu(1-s)]^{-1/b}}{\delta s}\right|_{s=1} = \mu \tag{6}$$

and

$$\sigma^2 = \left.\frac{\delta^2 Q(s)}{\delta s^2}\right|_{s=1} + \left.\frac{\delta Q(s)}{\delta s}\right|_{s=1} - \left[\left.\frac{\delta Q(s)}{\delta s}\right|_{s=1}\right]^2 = b\mu^2+\mu \tag{7}$$

The last result shows that the standard deviation depends upon the mean value, according to the relation $\sigma_{Py} = (b\mu^2 + \mu)^{1/2}$ for Polya distribution. For exponential distribution and Poisson distribution the dependence is given by relations: $\sigma_e = (\mu^2 + \mu)^{1/2}$ and $\sigma_{Po} = (\mu)^{1/2}$, respectively.

It follows that in the case of a Poisson distribution the standard deviation has the smallest value in comparison with standard deviation values of

Polya and exponential distributions for the same amount of the mean value in all three cases. Consequently, any departure from the Poisson distribution, in the secondary emission statistics, to Polya or exponential distribution degrades the single-electron pulse-height resolution, Fig. 1.[9a] The theoretically calculated multiple-particle pulse-height distribution for a two stage structure, with a very high gain second stage, using Polya statistics, gives twelve distinct electron peaks which are clearly resolvable[10], as it is shown in Fig. 2. However, for photomultipliers manufactured to date, our measurements show that the best electron resolution observed permitted the resolution of only 5 or 6 distinct electron peaks for conventionally designed photomultipliers[11]. Measurements were made according to the IEEE Standard Test Procedure for Photomultipliers for Scintillation Counting[11a]. The photoelectron pulse height spectrum obtained on a 400 channel pulse-height analyzer is shown in Fig. 3 for the RCA 8850 photomultiplier. Resolution of single electron peak which has a measured FWHM of 63% is shown in Fig. 4[6]. With a new prototype microchannel plate photomultiplier[12], eight or more distinct photoelectron peaks can be observed. However, such photomultipliers are not recommended for the DUMAND optical sensing array, because of significantly smaller photocathode quantum efficiency stability, and gain stability of presently available devices in comparison with conventional photomultipliers.

Generally, the first-electron resolution does not correlate very well with the first dynode gain for an effective dynode gain value larger than 30. Apparently, other mechanisms, as for example physical nonuniformities on the dynode surface which cause each element of the surface to have a different mean value for secondary emission, and nonuniformities of the collection efficiency of the first and second dynode[13], as well as other noise considerations from the photomultiplier and measuring system, may further degrade the electron resolution capabilities of the multi-stage photomultiplier.

Higher electron resolution capabilities, predicted by theoretical considerations of the secondary emission statistics, are possible if dynodes with better surface and collection efficiency uniformities than presently available, are produced.

Collection and Quantum Efficiency Uniformity Charactertistics

At the end of the 1980 DUMAND Workshop there was no decision about the particular photomultiplier which would be used in optical sensor modules. However, potential photomultiplier candidates should have a photocathode diameter of 5" or

larger. A cross section of a typical photocathode-to-first-dynode structure showing the input electron optics electrodes, equipotential lines and electron trajectories is shown in Fig. 5. In such a large photocathode area photomultipliers the collection and quantum efficiency uniformity can significantly vary as a function of the photocathode sensing area. Our measurements performed on an RCA C70133B, 5"-diameter photomultiplier with a cesium-activated gallium-phosphide secondary emitter, showed that the product of the collection and quantum efficiency varied within $^{+95\%}_{-45\%}$ for a distance of ± 55 mm from the center of the photocathode[11]. It can be seen from Fig. 6 that the largest variations occured at the edge of the photocathode, due primarily to reduced collection efficiency. The solid line shows the product of collection and quantum efficiency obtained when the photomultiplier was scanned with a 1.6 mm light spot in a direction parallel to the long direction of the first dynode and through the center of the photocathode. The dashed line is a result of scanning in a direction perpendicular to the first dynode. Similar results were reported for the Amperex 58AVP photomultiplier[14].

The collection efficiency varies with the potential distribution in the input electron optics and its value can be optimized for some photomultipliers. However, other photomultiplier characteristics may also vary with the potential distribution. For example, the potential distribution which maximizes collection efficiency does not necessarily minimize the single electron time spread[11]. Consequently, an optimization of photomultiplier operating conditions should be carried out for each type of photomultiplier intended for use in the DUMAND optical sensing modules following the procedure given in Ref. 11.

Electron Transit Time Difference and Electron Transit Time Spread Considerations

Electron transit time difference is the difference in transit time between electrons leaving the center of the photocathode and electrons leaving the photocathode at some specified point. In a typical photocathode design, the transit time is longer for edge illumination than for center illumination because edge trajectories are longer than axial trajectories, due to the weaker electrical field at the edge as it is shown in Fig. 5. Generally, transit-time difference information, although important, is not available from photomultiplier manufacturers.

The measured electron transit time difference as a function of the position of the photocathode sensing area along the X and Y axes for C70133B is shown in Fig. 7. It is interesting to note that the shapes of the electron transit

time difference curves, obtained from several tubes of the same type, are basically similar. Curves differ in details and in their maximum and minimum values. Added to the electron transit time difference is the transit time spread ultimately due to the initial-velocity distribution of emitted electrons from the photocathode.

The electron transit time spread of a photomultiplier is mainly caused by fluctuations of individual times of flight of photoelectrons and secondary electrons due to their different trajectories and their initial velocity difference. The factors that contribute to the transit time spread are differences in trajectory length and in electrical field strength for different portions of the photocathode-first-dynode region, and between various dynode sections. Generally, the amount of transit time spread depends upon photomultiplier geometric characteristics, its operating conditions, and the number of photoelectrons released from the photocathode. Since the time spread varies approximately inversely as the square root of the number of photoelectrons, the time behavior information of single photoelectrons is particularly helpful in predicting the transit time spread for an arbitary number of photoelectrons. Furthermore, it is also helpful in the evaluation, selection and comparison of photomultipliers, as well as in determination of photomultiplier optimum operating conditions in critical applications.

The total electron transit time spread of an electrostatically focused photomultiplier consists of the photoelectron transit time spread between the photocathode and the first dynode of the multiplier, the electron transit time spread in the electron multiplier, and that between the electron multiplier and anode. The major causes of transit time spreads are the distribution of initial emission velocities of photoelectrons and nonuniform electric fields. The initial stages of a photomultiplier contribute with the greatest weight to the total transit time spread. In the latter stages, the larger number of electrons in the pulse provide many samples of transit time through the stage and reduce the effect of transit time spread of that stages in the manner of the standard error of mean value. The variance of the total single photoelectron transit time t_σ^2, is approximately given by the following equation[15]

$$t_\sigma^2 \approx t_{CD1}^2 + \frac{t_{D1D2}^2}{g_1}(1 + g_{\sigma 1}^2) + \frac{t_{DD}^2}{g_1(g-1)}(1 + g_\sigma^2) \qquad (8)$$

where t_{CD1}^2 is the variance of the photoelectron transit time between the photocathode and the first dynode, t_{D1D2}^2 is the variance of the electron transit

time between the first and the second dynode, t_{DD}^2 is the variance of the electron transit time between two successive dynodes, g_1 is the gain of the first dynode, g is the gain of all other dynodes, $g_{\sigma_1}^2$ is the variance of the gain g_1, and g_σ^2 is the variance of the gain g.

The relation (8) shows that the total transit time variance will be considerably reduced using dynodes with emitting surfaces that have a high and uniform secondary emission yield. The total single photoelectron transit time spread, expressed by the full width at half maximum, is related to the standard deviation of the total transit time by the expression:

$$t_{\sigma FWHM} \approx 2.36 t_\sigma \tag{9}$$

The contribution to the transit time spread by the unequal electron path lengths between different electrodes and the nonuniformity of electric fields at the dynodes can be minimized by proper design of the input electron optics and the electron multiplier. This has been one of the goals of the photomultiplier manufacturers. Therefore, the ultimate limitation on time spread is determined by initial velocity effects of photoelectrons and secondary electrons. Assuming a uniform electric field between the photocathode and the first dynode, and equal photocathode-to-first-dynode electron path lengths, the time spread between a photoelectron emitted with zero initial velocity and a photoelectron with a velocity v_0 is approximately given by the equation[15]

$$\Delta t_n \approx \frac{v_0 l}{eV} m_0, \tag{10}$$

where l is the distance between the photocathode and the first dynode, V is the voltage between the photocathode and the first dynode, and e and m_0 are the charge and mass of an electron, respectively.

It can be seen from this equation that transit time spread resulting from the initial velocity distribution is decreased by increasing the voltage between the photocathode and the first dynode. Similar considerations are valid for the secondary electron initial velocity in an electron multiplier.

The single photoelectron time spread and time response of photomultipliers have improved considerably within the last few years, due both to better electro-optical design and to the application of new secondary emitters. Single photoelectron time spread is reduced in photomultiplier having dynodes

with GaP(Cs) secondary emitting surface, in comparison with conventional dynode emitter photomultipliers, because of the higher gain of individual dynodes in the multiplier structure and the reduced influence of the electron initial velocity differences. The larger number of emitted secondary electrons from the first dynode and the second dynode reduces the effect of electron transit time spread between the first dynode and the second dynode, as well as between the second and the third dynode. As a consequence, more possible electron paths are sampled in each pulse, and time spread caused by geometrical path considerations is reduced. Furthermore, secondary electrons from GaP(Cs) dynodes have a smaller spread in initial velocity, in comparison with conventional emitters. The remaining electron initial velocity differences are reduced by employing a high potential gradient at the emitting surface. In this case the electrons are more quickly accelerated to their terminal velocity, and initial electron velocity has a reduced influence on the total transit time and its spread. The practical limit for a maximum value of interstage potential differences is determined by field emission from the elements and electroluminescence of insulating materials. Both of these processes can increase the amount of the photomultipier dark current to an unacceptable level.

Single electron time spread as a function of the position of the photocathode sensing area along X and Y axes for C70133B, is shown in Fig. 8. It can be seen from the figure that the electron time spread variation is less than $^{+0.95}_{-1.30}$ ns within 55 mm of the center of the photocathode. With full photocathode illumination the single electron time spread, FWHM, was 2.42 ns. The single electron time spread spectrum is shown in Fig. 9. Larger values of the electron transit time difference and single electron time spread can be expected for photomultipliers with a hemispherical photocathode diameter larger than 5". Poorer secondary emitter materials, and smaller voltages between the photocathode and the first dynode will also degrade the time characteristics.

Afterpulses Considerations

Contemporary fabrication and activation techniques have reduced afterpulses from most photomultipliers to a point where they are rarely important. However, for the large photocathode area photomultipliers for the DUMAND detection system, a significant amount of afterpulses could be produced as a result of the ionization of residual gases, such as He, H_2, N_2 and CO, between the photocathode

and the first dynode. The positive ions formed are accelerated toward the photocathode by the focusing electric field. On impact, these ions liberate up to five secondary electrons which constitute the secondary signal or afterpulse. These afterpulses generally occur from 200 ns to several microseconds after the main pulse. The time of occurance of the afterpulses can be closely correlated with the atomic mass of the residual gas inside the glass envelope[16]. The EMI 9813 photomultiplier with a 2" diameter photocathode showed an afterpulse counting rate of 0.03% per photoelectron using a standard getter[17]. The afterpulse rate could increase significantly for 5" and 7" diameter photocathode photomultipliers. However, an application of a selective getter for the dominant gaseous impurity inside the glass envelope could reduce the afterpulse counting rate.

Effects of Ambient Magnetic Fields

Photoelectron trajectories between the photocathode and the first dynode are stongly influenced by relatively weak ambient magnetic fields. The effect on the photomultiplier gain is particularly strong because of a decrease of the collection efficiency, and it is always more critical in photomultipliers with large diameter photocathodes. For example, a magnetic field of 5 Gauss perpendicular to the major axis of the RCA 8055 photomultiplier, having a 5"-diameter photocathode, reduces the anode current for a factor of 10. For a direction of the magnetic field parallel to the major axis of the photomultiplier, the anode current would be reduced for approximately a factor of 4 for the same magnetic field intensity. Generally, the magnitude of the effect depends upon the structure of the photomultiplier, the orientation of the field, and the operating voltages. The effect of the field is smaller with the higher operating voltage.

The gain of the photomultipliers in the DUMAND optical sensing modules may be influenced by the earth's magnetic field and fields created by various cables carrying necessary power to the photomultipliers and data processing electronics which will be integrated into the DUMAND array. Consequently, magnetic shielding requirements for the optical sensing module photomultipliers should be determined after the DUMAND system is completely defined.

Stability of Photomultiplier Characteristics

The problem of photomultiplier life was considered at previous DUMAND workshops only in general terms, indicating a need for better understanding of

the aging mechanisms which cause photomultiplier failure[18,19]. The DUMAND array will have a minimum of 22,698 photomultipliers, and possibly two times that number, depending upon their configuration. Furthermore, assuming the DUMAND array component failures to occur and accumulate so that the array gradually deteriorates during its 10 year lifetime, the array end of life was defined as a failure (or loss of adequate sensitivity) for 30% of the 22,698 sensor modules. Consequently, it is important to estimate the photomultiplier reliability and its life.

According to the best knowledge of the author, no data on photomultiplier failure rates or life expectancy has been published for commericial, scientific, or military applications. The military specifications for the reliability of electronic receiving tubes cannot be applied to photomultipliers because of totally different failure mechanisms. Although adequate data has not been available in the open literature on photomultiplier life expectancy resulting from systematic studies, some preliminary studies have been made, particularly with respect to the photocathode lifetime. Also, there is operational experience in a number of National Laboratories where a large number of photomultipliers have been used in hodoscopes or detector configurations. Operational experience has shown that photomultiplier operational life is adversely affected by high current operation, excessive voltage operation, high photocathode illumination and high ambient temperature. In approaching this problem, it will be assumed that DUMAND array photomultipliers will be conservatively operated and that only a slow deterioration of photomultiplier characteristics will take place. In this case, the photocathode is the most critical part of a photomultiplier, followed by the electron multiplier.

Concerning the photocathode stability, it has been shown that the photocathode quantum efficiency steadily decreases with the operating time even when the photomultiplier is conservatively operated[20-22]. There is also a change in shape of the spectral response characteristics. The rate of the decrease varies with operating time.

Experiments performed by various authors as well as our own measurements made on photomultipliers using special measuring systems[23] show that a degradation of the quantum efficiency and a change in shape of the spectral response characteristics are essentially caused by the positive ions which are present inside the vacuum envelope and are then continually accelerated back to the photocathode. Electrolytic processes between the photocathode and its substrate, and

the photocathode temperature contribute to photocathode degradation. The deterioration of the photocathode because of an electrolytic process through glass can result from the proximity of a high potential gradient in the region of the photocathode. Such a gradient can occur when the photomultiplier is operated with the anode near ground potential. Magnetic shield at ground potential may provide the contact needed for such a gradient through the glass near the photocathode With an appropriate designing technique, this effect can be minimized or completely eliminated. The photocathode deterioration processes are deaccelerated as the temperature decreases. The DUMAND photomultipliers will operate at ambient temperatures of approximately 0°C which should reduce photocathode deterioration in comparison with room temperature operation.

Measurements made on three ITT F4052 image dissectors[20] with the S25 photocathode showed a photocathode sensitivity decrease to an average of approximately 42% from its initial value in the first 7000 hours of operating time, using a Corning CS-5-58 (blue) filter. The sensitivity decrease was 97% for the same operating time interval, was measured using a Corning CS-2-62 (red) filter. The lifetime measurement was done with a constant illumination and initial photocathode current density of approximately 3 $\mu A/cm^2$. This current density is significantly higher than one would expect for photomultiplier operation in the DUMAND array. Generally, for a higher photo-current density, the more rapidly the photocathode sensitivity decreases with time.

Measurements made on twenty ITT F 4012 image dissectors with S11 photocathodes showed a sensitivity decrease of approximately 38% from its initial value for the first 7000 hours of operating time at 4080Å wavelength and a decrease of 52% when measured at 6130Å wavelength. Again, a constant illumination was used for all measurements with an initial photocathode current density of 1 $\mu A/cm^2$ and the image section voltage of 400 V. A preliminary conclusion is that under constant illumination the photocathode sensitivity decrease curve is approximately an exponential decay with time. Initially, the rate of change of the sensitivity is quite large. However, as time goes on the rate greatly decreases. The photocathode itself very rarely fails catastrophically. Furthermore, for a given period of time the S25 photocathode could have the longest useful life, because it generally starts with a higher sensitivity and does not decrease appreciably faster than the other types.

Photomultipliers for the DUMAND sensor modules, should have the fast acting getters, with pumping speed considerably higher for residual gases inside the

vacuum envelope than the speed with which the photocathode accepts contamination. Also, the input electron optics potentials should be optimized as to minimize the damage of the photocathode due to residual gas positive ions.

Measurements of the relative spectral sensitivity of photodiodes with those S10 photocathodes showed that there is similar change during the first three years of life[24]. The aging process leads to a greater loss of red sensitivity than blue.

Concerning the electron multiplier gain stability and fatigue phenomena, measurement has shown that they are a function of the anode output current level, dynode materials, and operating time. For a high gain stability, the average anode current should be as small as possible to reduce the erosion of the dynodes by electron bombardment. Electron multipliers using copper beryllium dynodes have shown more stable gain particularly when operated at higher temperatures, than cesium antimony ones. A slow decrease of the photomultiplier gain in the DUMAND sensor module can be easily and continuously corrected by an appropriate feedback system.

Based on the above given considerations and experience with photomultiplier reliability obtained from several National Laboratories, the large photocathode areas photomultiplier will satisfy the DUMAND array lifetime requirements. This assumes that they are manufactured under conditions of strict quality control, and that they are screened and selected. Also, to increase reliability, the photomultiplier operating conditions in the DUMAND array should be optimized for a maximum lifetime.

Acknowledgements

This work was performed as part of the program of the Electronics Research and Development Group of the Lawrence Berkeley Laboratory, University of California, Berkeley, and was partially supported by the High Energy Physics Division of the U. S. Department of Energy under contract No. W-7405-ENG-48.

References

1. A. Roberts, G. Wilkins, The 1978 DUMAND "Standard" Array. Proceedings of the 1978 DUMAND Summer Workshop, Vol. 3, pp 9-22*

2. H. Hinterberg, A. Roberts, F. Reines, Improvements in the 1978 Standard DUMAND Module: Sea Urchin, Proceedings of the 1979 DUMAND Workshop held in Khabarovsk, Siberia, U.S.S.R.

3. J. G. Learned, Trigger Rate Considerations for the 1978 DUMAND Summer Study Model Array, Proceedings of the 1978 DUMAND Summer Workshop, Vol. I, pp 147-163*.

4. A. Roberts, Potassium 40 in the Ocean and How to Live With It. Proceedings of the 1978 DUMAND Summer Workshop, Vol. 1, pp 139-145*.

5. R. E. Simon and B. F. Williams, Secondary-Electron Emission, IEEE Trans. Nucl. Sci., NS-15, No. 3, pp 167-170 (1968).

6. G. A. Morton, H. M. Smith, and H. R. Krall, The Performance of High-Gain First-Dynode Photomultipliers, IEEE Trans., Nucl. Sci., NS-16, pp 92-95, (1969).

7. H. R. Krall, F. A. Helvy, and D. E. Gersyk, Recent Developments in GaP(Cs) Dynode Photomultipliers, IEEE Trans. Nucl. Sci., NS-17, No. 3, pp 71-74, (1970).

8. W. Feller, in Introduction to Probability Theory and Its Applications, Vol. 1, (Wiley, New York, 1957).

9. J. R. Prescott, A Statistical Model for Photomultiplier Single-Electron Statistics, Nucl. Instr. Methods, 39, 173-179 (1966).

9a. RCA Photomultiplier Manual, Technical Series PT-61, 1970, RCA Corporation (Electronic Components), Harrison, N. J., 07029.

10. L. A. Dietz, Use of Polya Statistics in Investigations of Secondary Electron Yields from Target Surfaces, Rev. Sci Instr., 38, No. 9, 1332-1333, (1967).

11. B. Leskovar, C. C. Lo, Performance Studies of Photomultipliers Having Dynodes with GaP(Cs) Secondary Emitting Surface, IEEE Trans. Nucl. Sci., NS-19, No. 3, pp 50-62 (1972).

11a. IEEE Standard Test Procedures for Photomultipliers for Scintillation Counting and Glossary for Scintillation Counting Field, IEEE Standard 398-1972 (American National Standards N429-1972) Available from Standard Office, Institute of Electrical and Electronics Engineers, 345 East 47th Street, N.Y., N.Y., 10017.

12. C. C. Lo, B. Leskovar, Studies of Prototypes High-Gain Microchannel Plate Photomultipliers, IEEE Trans. Nucl. Sci., NS-26, No. 1, pp 388-394 (1978). LBL-7957.

*Published by DUMAND Scripps Institution of Oceanography, Code A-010, La Jolla, CA.

13. Private communication with T. T. Lewis, February 1972, RCA Corporation, Lancaster, Pennsylvania.

14. J. M. Paul, Studies Concerning the Behavior of Photomultipliers with Large Photocathodes, Nucl. Instr. and Methods, 89, pp 285-287, Dec. 1, (1970).

15. B. Leskovar, and C. C. Lo, Single Photoelectron Time Spread Measurement of Fast Photomultipliers, Nucl. Instr. Methods, 123, pp 145-160 (1975).

16. G. A. Morton, H. M. Smith, R. Wasserman, Afterpulses in Photomultipliers, IEEE Trans. Nucl. Sci., NS-14, No. 1, pp 443-448, (1967).

17. A. G. Wright, Sources of Noise in Photomultipliers, EMI Report RIP068, 1977, EMI Electron Tubes, Division of EMI Industrial Electronics Ltd., Middlesex, England.

18. S. J. Cowen, G. D. Gilbert, J. T. Redfern, Array Electronics and Signal Processing, Proc. of the 1978 DUMAND Summer Workshop, Vol. 3, pp. 97-119*.

19. C. R. Gundersen, Maintenance of the DUMAND Array, Proc. of the 1978 DUMAND Summer Workshop, Vol. 3, pp 161-169*.

20. R. J. Hertel, Photocathode Life Tests (Vidisector) Technical Note 114, Electron Tube Division-ITT, April 1970.

21. D. McMullan, J. R. Powel, Residual Gases and Stability of Photocathodes, Advances in Electronics and Electron Physics, Vol. 40A, pp 427-439, 1976.

22. B. Leskovar, C. C. Lo, Stability of Microchannel Plate Photomultiplier Characteristics--Some Preliminary Results, Lawrence Berkeley Laboratory Engineering Note EE-1481, April 18, 1977.

23. C. C. Lo, B. Leskovar, A Measuring System for Studying the Time Resolution Capabilities of Fast Photomultipliers, IEEE Trans. Nucl. Sci., NS-21, No. 1, pp 93-105, (1974).

24. W. Budde, Aging of S-10 Photocathode, Applied Optics, Vol. 12, No. 9, pp 2108-2114, September 1973.

*Published by DUMAND Scripps Institution of Oceanography, Code A-010, La Jolla, CA.

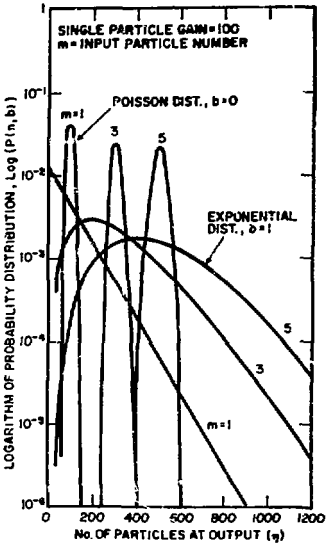

Fig. 1 A comparison of multiple-particle distributions from a single dynode having Poisson and exponential distribution.

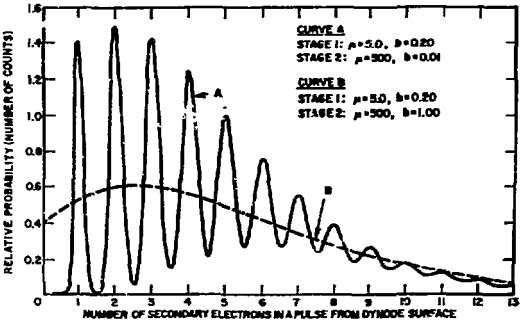

Fig. 2 Theoretical pulse-height distributions. Stage gain is μ, and b is a parameter associated with a Polya distribution. For instance, b-values of zero and unity represent Poisson and exponential pulse-height distributions, respectively. The mean value of all two distributions is normalized to coincide with that of 5 electrons from the target surface. This is assumed to be the gain of the first stage. Ordinate values for the one-stage and two-stage cases are normalized by multiplying the probability coefficients by the gain of one and two stages, respectively.

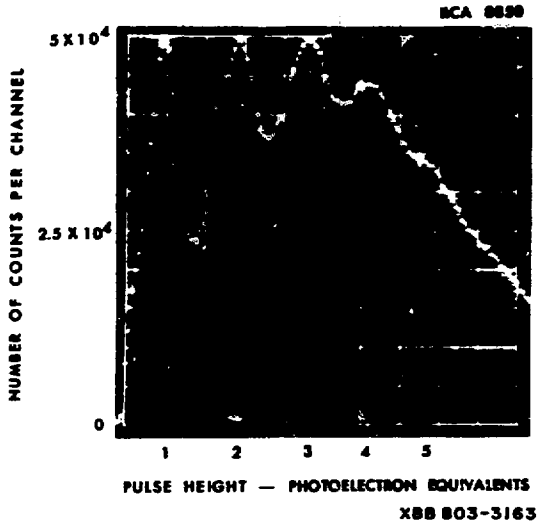

Fig. 3 Pulse-height spectrum, showing peaks corresponding to one, two, and up to five electron peaks, for RCA 8850 photomultiplier.

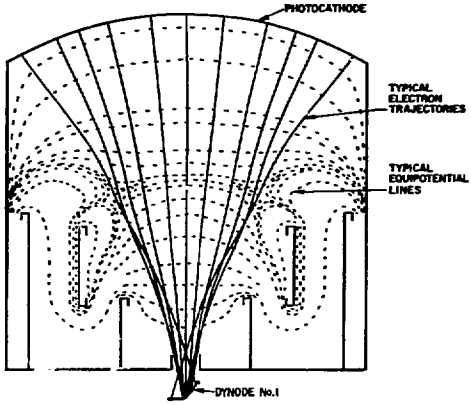

Fig. 5 Cross section of a photomultiplier showing equipotential lines and electron trajectories.

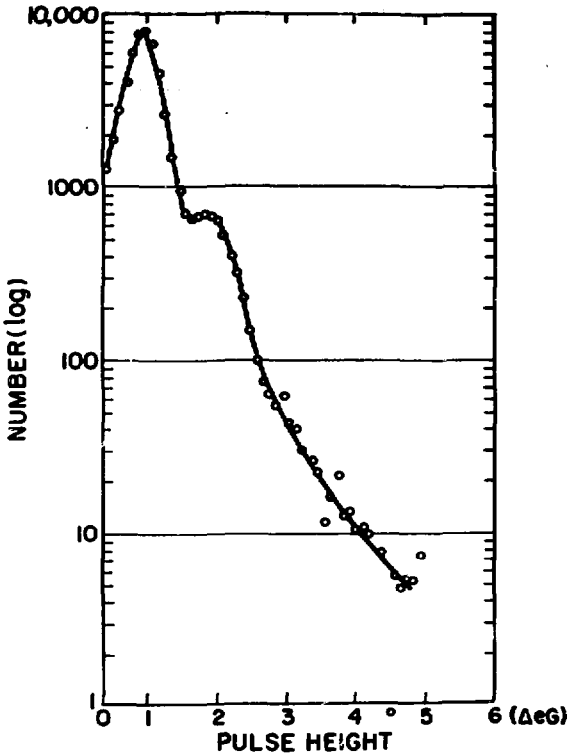

Fig. 4 Resolution of a single electron peak which has a measured FWHM of 63%.

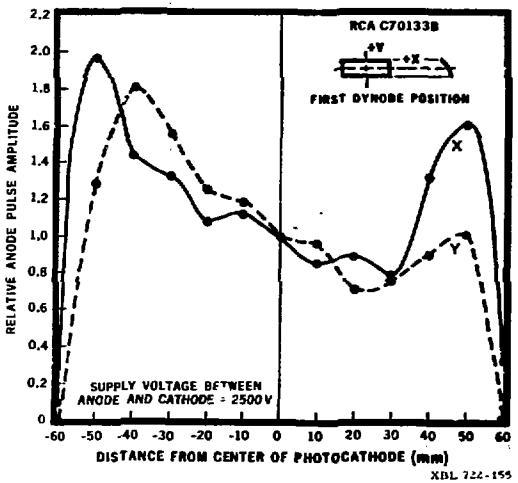

Fig. 6 Collection and quantum efficiency uniformity as a function of the position of the photocathode sensing area, for RCA C70133B photomultiplier.

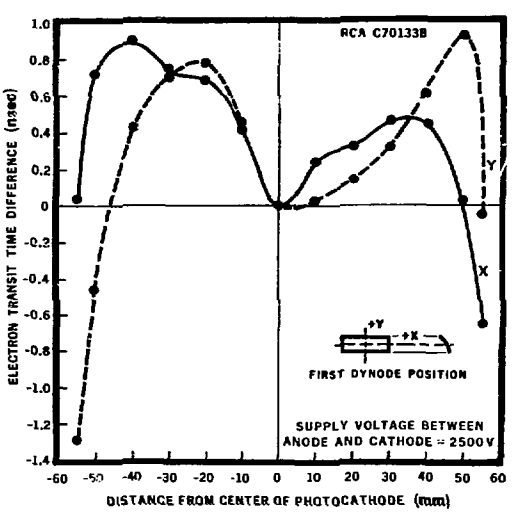

Fig. 7 Electron transit time difference as a function of the position of the photocathode sensing area for RCA C70133B photomultiplier.

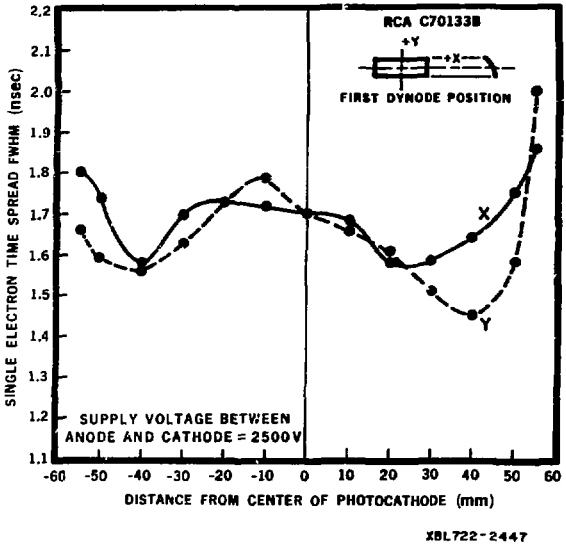

Fig. 8 Single electron time spread as a function of the position of the photocathode sensing area for RCA C70133B photomultiplier.

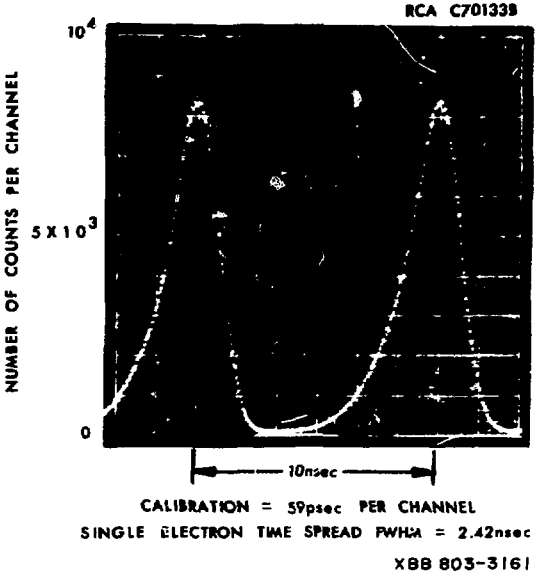

Fig. 9 Single electron time spread of RCA C70133B photomultiplier with full photocathode illumination.